Environmental Earth Sciences (2021) DOI: https://doi.org/10.1007/s12665-021-09527-4
Received: 23 May 2020 / Accepted: 4 March 2021

Source of ^{226}Ra in Ramsar Springs Water, Iran: Implication of Water–Rock Interaction and Stable Isotopes

Farideh Amini Birami[1]*, Farid Moore[1]*, Mohammad Reza Kardan[2], Behnam Keshavarzi[1], Mehdi Zarei[1], Peter S. Hooda[3]

[1] *Department of Earth Sciences, College of Sciences, Shiraz University, Shiraz, Iran*

[2] *Nuclear Science and Technology Research Institute, Tehran, Iran*

[3]*School of Geography, Geology and the Environment, Kingston University London, Kingston Upon Thames KT1 2EE, UK*

* Corresponding author:
amini-birami@shirazu.ac.ir
farid1328@gmail.com

Source of ^{226}Ra in Ramsar Springs Water, Iran: Implication of Water–Rock Interaction and Stable Isotopes

Abstract

This study was carried out primarily to understand the hydrogeochemical processes controlling the ^{226}Ra anomalies in Ramsar area. Analyses revealed two types of water; 1) non-thermal Ca-HCO_3 type and 2) thermal Na-Cl type, mainly of meteoric and hydrothermal origin, respectively. Non-thermal springs have higher concentrations of U due to silicate weathering. Thermal springs are characterized by high concentrations of ^{226}Ra, As, Fe, Li, Cs, Rb, Sr, Ba, B, Br^-, F^-, NO_3^-, PO_4^{3-} and SiO_2 resulting from high temperature water-rock interaction and mixing with hydrothermal fluids. Thermal springs are manifestations of an old hydrothermal system with subsurface reservoir temperatures varying between 83 and 100°C. Radium activity is negatively correlated with pH and positively correlated with TDS, Cl^-, Ba, and Ca, reflecting competitive ion effects of alkaline-earth metals, complexing with Cl^-, and co-precipitation with barite and calcite. These processes are thought to be the dominant factors in controlling ^{226}Ra mobility in springs water.

Keywords: radium; water–rock interaction; hydrogeochemistry; stable isotops; Ramsar

1. Introduction

Naturally occurring radionuclides fall within those scientific subjects that attract public attention, due to their significant role in most external radiation exposure (Bozkurt et al. 2007; Tabar et al. 2013). Long-term exposure to these radionuclides could lead to many health problems; including leukopenia, anemia, and leukemia as well as lung, pancreatic, liver, bone and kidney cancers (Qureshi et al. 2014). Radionuclides are naturally omnipresent on Earth in various concentrations. In most areas, their activity concentration differs within narrow ranges, but in high background radiation areas, they occur at greater than normal concentration (2.4 mSv/year) (UNSCEAR 2000). High background radiation areas are already reported from Guarapari in Brazil (Paschoa 2000), Yangjiang in China (Tao et al. 2012), Kerala in India (Nair et al. 2009), and Ramsar in Iran (Khademi and Tahsili 1972). The main source of background radiation in Ramsar is ^{226}Ra and its decay products. Ramsar has been the subject of various radiobiological and epidemiological studies for decades (Amini Birami et al. 2019, 2020; Fathabadi et al. 2017, 2019; Ghiassi-Nejad et al. 2002; Khademi and Mesghali 1971; Khademi et al. 1980; Khademi et al. 1975; Shorabi 1990; Sohrabi and Esmaili 2002; Sohrabi and Babapouran 2005; Sohrabi 2013). The results indicate that, the inhabitants of some areas in Ramsar are exposed to radiation higher than the recommended 20 mSv/y limit for radiation workers. Furthermore, the highest worldwide calculated annual effective dose to humans (260 mSv/y) also comes from this area (Ghiassi-Nejad et al. 2002; Sohrabi and Babapouran 2005). Radium-226 is a product of ^{238}U decay chain with a half-life of 1620 years. Uranium forms a soluble carbonate complex under oxic conditions, and is transported by water over long distances; and precipitates, under anoxic condition. Consequently, produced Ra distributes widely in aqueous systems (Michel 1990). A proposed hypothesis suggests that ^{226}Ra anomalies in Ramsar are the result of thermal spring interaction

with subsurface uraniferous igneous rock bodies (Ghiassi-Nejad et al. 2002). As it happens, none of the previous surveys coupled data on ^{226}Ra occurrence with extensive hydrogeochemical information of springs water to determine the source of ^{226}Ra in Ramasr. Thus, investigating the processes and factors that control ^{226}Ra activity in springs water is of scientific and practical importance. The primary aim of this study is to conduct a detailed evaluation of the hydrogeochemical properties of springs water in the vicinity of Ramsar area to better understand the source of ^{226}Ra activity in the springs water.

2. Study area description

The study area is located north of Iran between the Caspian Sea shoreline and the Alborz Mountains foothills N36°59′ to N36°21′ and E50°30′ to E51°12′ (Fig. 1). Geologically, the Alborz Mountains range is an E-W-striking intracontinental orogen in north Iran representing a small portion of the northern border of the Alpide collision belt. Alborz Mountains are the result of relative movement between the stable South Caspian Basin, and the Central/Eastern Iranian blocks. The Alborz joins Caucasus Mountains to the northwest and is confined by Hindu Kush mountains to the east (Zanchi et al. 2006). The Alborz rifted from Gondwana during Ordovician to Silurian period and collided with the Eurasia in Triassic period (Alavi 1996; Stampfli 2000). Therefore, Alborz is considered to be an active mountain belt resulting from Gondwana and Eurasia plate collision in Triassic (Guest et al. 2006) In this area, extensional deformation phases were initiated with the incidence of late Triassic rift volcanism and the deposition of carbonaceous shales and coals of Shemshak Formation. Collision between Arabian and Eurasian plates took place in Triassic period during Mesozoic era (Berberian et al. 1982). During late Jurassic and early Cretaceous periods shallow marine carbonates deposited along with associated alkaline basalts eruptions (Nazari and Shahidi 2011). The oldest formations in the study area are Kahar schists and slates (Precambrian) (Alavi, 1996). In the study area, Permain limestone and sandstone unites encompassed by volcanic and pyroclastic basaltic to andesitic units (Vahdati Daneshmand 2004). Massive dolomites of Elika Formation (Triassic) along with interlayers of basaltic rocks represent lower Mesozoic era. The shaly layers of Shemshak Formation (Jurassic) overlap with Precambrian, Upper Triassic, and Middle Triassic units along an angular unconformity (Cartier 1971). To the south of the study area, the emplacement of three granitic intrusions (Arud, Noosha, and Akapol) is reported with the age of Paleocene and Oligocene epochs (Vahdati Daneshmand et al. 2001). The spatial distribution of geological units in a decreasing order of age are presented in Fig. 1.

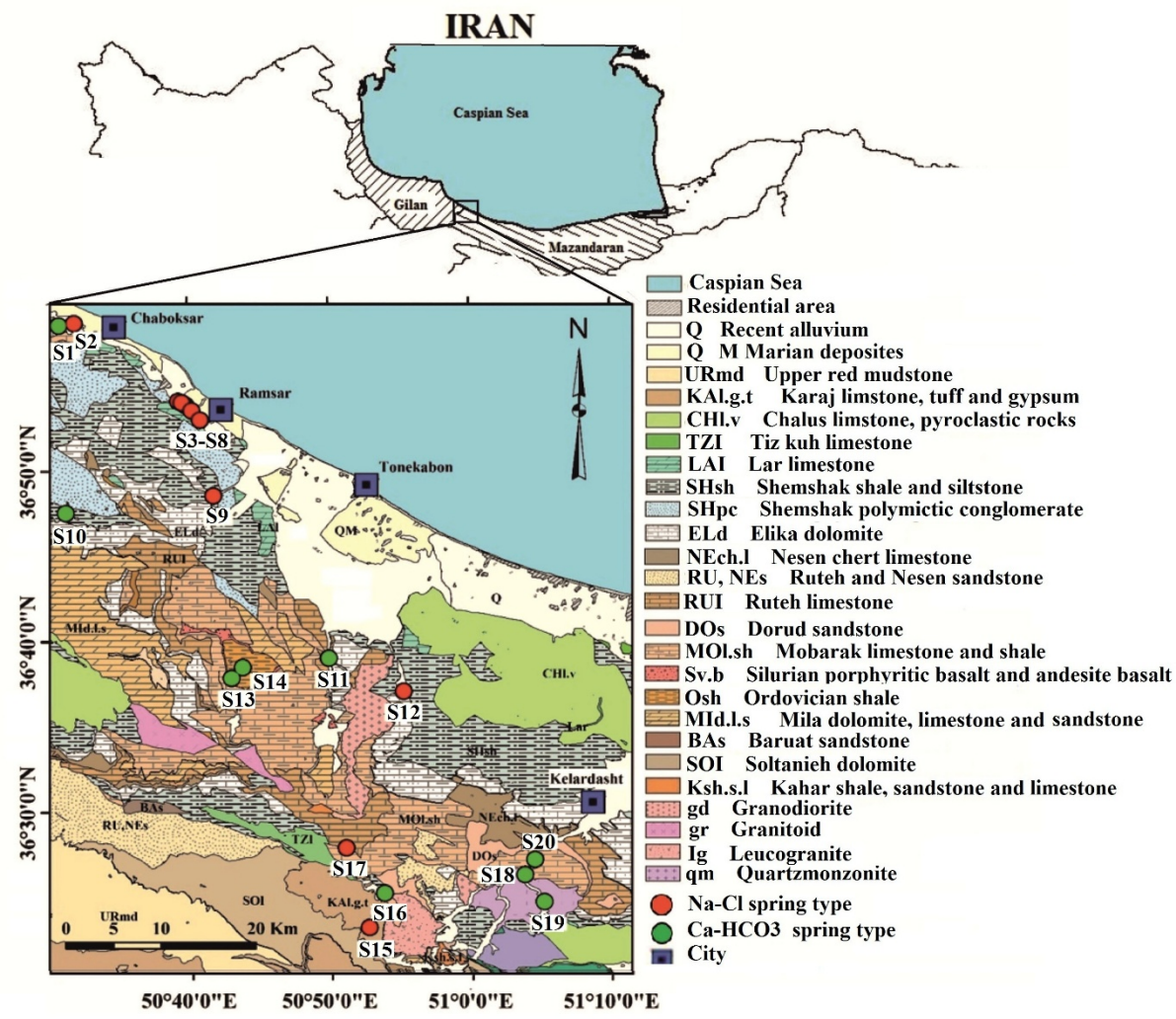

Fig. 1. Geological formations and spatial distribution of the springs water sampling stations showing water type.

The climate is predominantly humid to sub-humid subtropical. The average annual rainfall is 1500 mm with an average annual temperature of 17 °C. The warmest and the coldest months of the year are August (average temperature of 25 °C) and February (average temperature of 8 °C), respectively. The Caspian Sea level stands 27 m below m.s.l. The general direction of groundwater flow is northward, from the Alborz Mountain range towards the Caspian Sea (Sheikhy et al. 2014). Groundwater table, near the foothills of the Alborz Mountains, is at an altitude of 106 m above m.s.l, which slopes down towards the Caspian Sea. The water table is shallow along the shoreline standing approximately 25 m below m.s.l (Khairy et al. 2013). The aquifer in the coastal plain constitutes four layers from top to bottom as follows: a) an unconfined aquifer of gravel, sand, and calcareous components; b) an aquitard of clay, sandy clay, and silty clay; c) a semiconfined aquifer composed of calcareous gravel, sand, and silt and d) a marine sandy and silty unit. All unites contain noticeable amounts of marine shells (Alavi 1996; Khairy et al. 2013).

3. Sampling and analytical methods

Twenty spring water samples were collected from various springs in the study area (Fig. 1). Six spring water samples (S3, S4, S5, S6, S7, and S8) were collected in the vicinity of Ramsar city and the rest from separated rural districts. The characteristics of the springs are presented in Table S1. Physicochemical parameters including pH, oxidation reduction potential (ORP), and temperature were quantified using a multiparametric Eutech portable meter (model PCD 650). ORP values were determined using silver chloride electrode and changed to Eh values by changing for the reference electrode (Amini Birami et al. 2020). Total dissolved solid (TDS) load was measured by evaporation. Chloride and bicarbonate were determined using $AgNO_3$ and acid titration methods, respectively. Sodium and potassium were measured using a flame photometer (PFP7, Jenway). Calcium and magnesium were measured by titration with EDTA. Sulfate, nitrate, bromide, fluoride, phosphate and silica were analyzed using spectrophotometry (DR/2500, Hach, USA) (APHA 1995). All measurements were performed in the Hydrochemical Laboratory of Shiraz University, Iran. All calculated charge balance were less than ±5%. The detection limits were below, 0.1 meq/L for Cl^-, HCO_3^-, Ca and Mg, 0.01 meq/L for Na^+, K^+ and 0.01 mg/L for SO_4^{2-}, NO_3^-, Br^-, F^-, PO_4^{3-} and SiO_2. To analyze trace elements, all water samples were filtered through 0.45 µm syringe filters to separate suspended solids. Then, samples were acidified (pH<2) by ultrapure HNO_3. The concentrations of As, Fe, Li, Rb, Sr, Cs, Ba, B, and U were measured using inductively coupled plasma mass spectrometry (ICP-MS) in Activation Laboratories Ltd. Ontario, Canada. Quality assurance and quality control of analyses were done checked using analytical replicates, duplicates, blank reagents, and confirmed reference material (IV-STOCK-1643). The mean recoveries of trace elements were in the range of 96–115% and the relative standard deviation was less than 5%. The detection limits were below, 0.001 µg/L, for Cs and U, 0.005 µg/L for Rb, 0.03 µg/L for As, 0.04 µg/L for Sr, 0.10 µg/L for Ba, 1 µg/L for Li, 3 µg/L for B, and 10 µg/L for Fe.

Spring water samples for ^{226}Ra measurement were filtered through a 0.45 µm vacuum pump filters and acidified (pH<2) using ultrapure HNO_3 and transferred to pre-washed 1-L polyethylene Marinelli beakers. Then, the beakers were sealed for a month to attain the secular equilibrium. The concentration of ^{226}Ra was measured using gamma spectroscopy equipped with p-type coaxial high-purity germanium detector in Radiation Research Center of Shiraz University, Iran, with a relative efficiency of 40% and resolution of 1.90 keV for the 1332.5 keV gamma ray emission of Cobalt-60.

Energy calibrations were carried out by calibrating point sources (^{241}Am, ^{133}Ba, ^{137}Cs and ^{60}Co) (Knoll 2010; ASTM 2004). The efficiency calibration of the gamma spectrometer was performed using multinuclides standard solutions prepared by International Atomic Energy Agency (IAEA). One pre-washed Marinelli beaker filled with distilled water was used to strip the values of background radiation value, while standard samples were applied for quality assurance. The spectrum of each sample was recorded for 72 hours. The activity of ^{226}Ra was obtained according to gamma ray energies of ^{214}Pb (295.22 and 351.93 keV) and ^{214}Bi (609.31, 1120.29 and 1764.49 keV). The minimum detectable activity of the system for ^{226}Ra was 0.30 Bq/L (ASTM 2004).

Springs water samples for stable isotopes ($\delta^{18}O$ and δD) were analyzed by a los gatos research (LGR) laser system. For this purpose, 1000 nL of spring water was placed into the heated septum port by a LEAP

Technology (CTC) PAL liquid autosampler. Then, the vaporized water samples expanded into the laser cell of the LWIA. Each sample was injected 8 times. The first 2 times were ignored but the remaining 6 times were averaged for reporting. The H_2O molecules were analyzed by Off-Axis Integrated-Cavity Output Spectroscopy (ICOS) Laser System. The results are reported in the standard δ-notation with respect to the Vienna Mean Ocean Water (V-SMOW) standard. The analytical precision of stable isotope measurements was ±0.8‰ for δD and ±0.2‰ for $\delta^{18}O$.

4. Results and discussion

4.1. Physicochemical parameters and chemistry of springs water

The results of the physicochemical and chemical measurements are shown in Table S1 and summary of descriptive statistics of the measured parameters are presented in Table 1. In this study, all values below the detection limit (<LOD) were taken as 75% of the detection limit. Piper diagram (Piper 1953) shows that the investigated spring water samples are of two hydrochemical types of Na-Cl and Ca-HCO_3. No spring water displayed a chemical composition similar to that of the Caspian Sea (Fig. S1). The temperature varied from 25 to 47°C with a median of 32.50°C for Na-Cl water type springs and 10 to 17°C with a median of 13.5°C for Ca-HCO_3, water type springs. Na-Cl type springs (S2, S3, S4, S5, S6, S7, S8, S9, S12, S15, and S17) and Ca-HCO_3 type springs (S1, S10, S11, S13, S14, S16, S18, S19, and S20) were categorized as thermal (T>21°C) and non-thermal springs (T<21 °C), respectively (Meinzer, 1923). pH varied from 6.10 to 7.24 with a median of 6.58 for thermal springs and 6.18 to 9.15 with a median of 7.76 for non-thermal springs. Also, Eh ranged from 9.3 to 368 mV with a median of 90 mV for thermal springs and 280 to 322 mV with a median of 300 mV for non-thermal springs. TDS ranged from 0.40 to 102 g/L with a median of 16 g/L for thermal springs and 0.10 to 0.85 g/L with a median of 0.20 g/L for non-thermal springs.

The average TDS of the Caspian Sea water along the southern coast is less than 15 g/L (Pervov et al. 2003). In the study area, S3 and S7 springs should be classified as brine (TDS>100 g/L), S4, S5, S6 and S8 as saline water (10<TDS<100 g/L), and S2, S9, S12, S15 and S17 as slightly brackish water (1<TDS<10 g/L) (Todd 2005). The lowest pH and Eh, and the highest TDS values were measured in Ramsar's thermal springs. The median concentration of Li, Cs, Rb, Sr, Ba, B, Br^-, F^-, NO_3^-, PO_4^{3-} and SiO_2, in thermal springs is higher than non-thermal springs (Table 1), indicating that they are sourced from deep reservoirs with high temperature water-rock interactions (Chatterjee et al. 2017, Sherif et al. 2018, Wrage et al. 2017). Saturation index of minerals was calculated using PHREEQC Interactive V. (3.3.12) based on Pitzer and IInI database for thermal and non-thermal springs, respectively (Parkhurst and Appelo 2013).

4.2. Mechanisms controlling springs water chemistry

The relationships between the main constituents of water samples were used to distinguish the influence of various processes on their hydrochemistry. Sodium and chloride in halite structure occur at equal concentrations. The Na^+/Cl^- ratio (meq/L) varied from 0.86 to 1.68 with a median of 0.95 in the thermal springs and 0.24 to 7.25 with a median of 0.92 in the non-thermal springs. All samples proved to be undersaturated with respect to halite (Table S2), indicating that they have not been in equilibrium with halite (Belhai et al. 2016). As shown in Fig. 2a, most of the springs are located below the halite dissolution line, revealing that Na^+ concentrations are lower than Cl^-. In hydrothermal systems, Cl^- acts as the main

ligand for the cations transfer. Therefore, additional Cl^- in thermal springs may have originated from mixing with hydrothermal fluids (Pirajno 2013) and/or dissolution of late-stage evaporite minerals (Vengosh et al. 1998). The molar ratio of Li^+/Cl^- in the thermal springs reiterate from 1.05E-04 to 1.20E-02 with a median of 2.05E-03. These values are higher than reported ratio range for halite dissolution by Zarei et al. (2013) (1.0E-05 – 5.0E-05) and Kloppmann et al. (2001) (1.0E-04 - 6.0E-06). The high ratio of Li^+/Cl^- in thermal springs confirms the influence of hydrothermal water-rock interactions on the springs water chemistry (Saou et al. 2012). Furthermore, the Br^-/Cl^- molar ratio of the thermal springs varied from 1.66E-04 to 7.09E-04 with a median of 4.67E-04. These values are lower the than seawater ratio (1.57E-03) (Hounslow 2018). Therefore, the composition of thermal springs seems to be affected by mixing with hydrothermal fluids and secondary brines.

Table 1. Statistical summary of physicochemical parameters, chemical and isotopic composition of the two spring water samples.

Parameter	Unit	Range	Mean	Median	Range	Mean	Median
		Thermal Springs (n=11)			Non-thermal Springs (n=9)		
T	°C	24-48	32.5	32.40	10.50-16	13	13.50
pH		6.10-7.24	6.67	6.58	6.18-9.15	7.83	7.76
Eh	mV	9.30-367	172	89	279.30-321.70	302	301
TDS	g/L	0.42-103.33	28.90	15.80	0.11-0.85	0.31	0.22
EC	mS/cm	3.37-187	49.84	26.41	0.17-2.41	0.64	0.37
Ca^{2+}	meq/L	3.42-225	59	40.30	1.1-16	5.38	2.75
Mg^{2+}	meq/L	1.53-55	16.28	10	0.25-2.20	1.45	1
Na^+	meq/L	27-1800	467	222	0.05-6	1.16	0.18
K^+	meq/L	0.05-8.03	2	1.10	0.01-0.18	0.07	0.04
HCO_3^-	meq/L	4.50-17.50	12	12.50	1.50-20	6.15	3
Cl^-	meq/L	17-2050	524.27	250	0.15-6.50	1.14	0.25
SO_4^{2-}	meq/L	0.05-6	2.17	1.5	0.05-2.25	0.32	0.07
As	µg/L	<LOD -164	17.82	1.53	0.07-476	53.30	0.44
Fe	µg/L	<LOD -90	32.27	7.50	20-44	34	36
Li	µg/L	11-1820	678.36	346	<LOD	-	-
Cs	µg/L	1.68-166	39.40	21.10	<LOD -62.50	11.06	0.08
Rb	µg/L	11.80-373	160.27	133	0.17-342	48.20	1.11
Sr	µg/L	1570-211000	54563.64	22300	95-3730	613.11	196
Ba	µg/L	27.10-54700	9845.05	406	15.60-55	40.08	38.90
B	µg/L	31-28100	7837.18	3960	2.25-1790	266.80	17
U	µg/L	<LOD -0.90	0.18	0.06	<LOD -4.02	0.98	0.74
Br	mg/L	0.60-104.87	22.60	10.20	<LOD	-	-
F^-	mg/L	0.05-2.58	1.45	1.63	<LOD -1.720	0.37	0.24
PO_4^{3-}	mg/L	0.75-58.35	12.50	5.22	1.50-24.86	6.78	4
NO_3^-	mg/L	0.04-3.75	0.52	0.13	0.05-0.60	0.17	0.10
SiO_2	mg/L	24.10-180.80	61.38	52.30	6.40-99.50	19.72	10.50
^{226}Ra	Bq/L	<LOD -65	13.30	1.56	<LOD -0.45	0.30	0.22
$\delta\ ^{18}O$	‰	-11.68-(-6.29)	-8.95	-9.22	-11.20-(-8.20)	-9.96	-9.97
$\delta\ D$	‰	-73.56-(-48.97)	-61.18	-63.20	-69.86-(-46.18)	-60.83	-60.12

LOD : limit of detection

The low values of Na^+/Cl^- ratio (in meq/L) in the non-thermal springs can be interpreted as reflecting dissolution of late-stage evaporates, such as KCl and $CaCl_2$ (Vengosh et al. 1998). Reverse ion exchange

process and conversion of plagioclase and/or K-feldspar into albite and/or analcime are two likely processes that might reduce the concentrations of Na^+ in springs water (Alçiçek et al. 2016; Hounslow 2018).

-

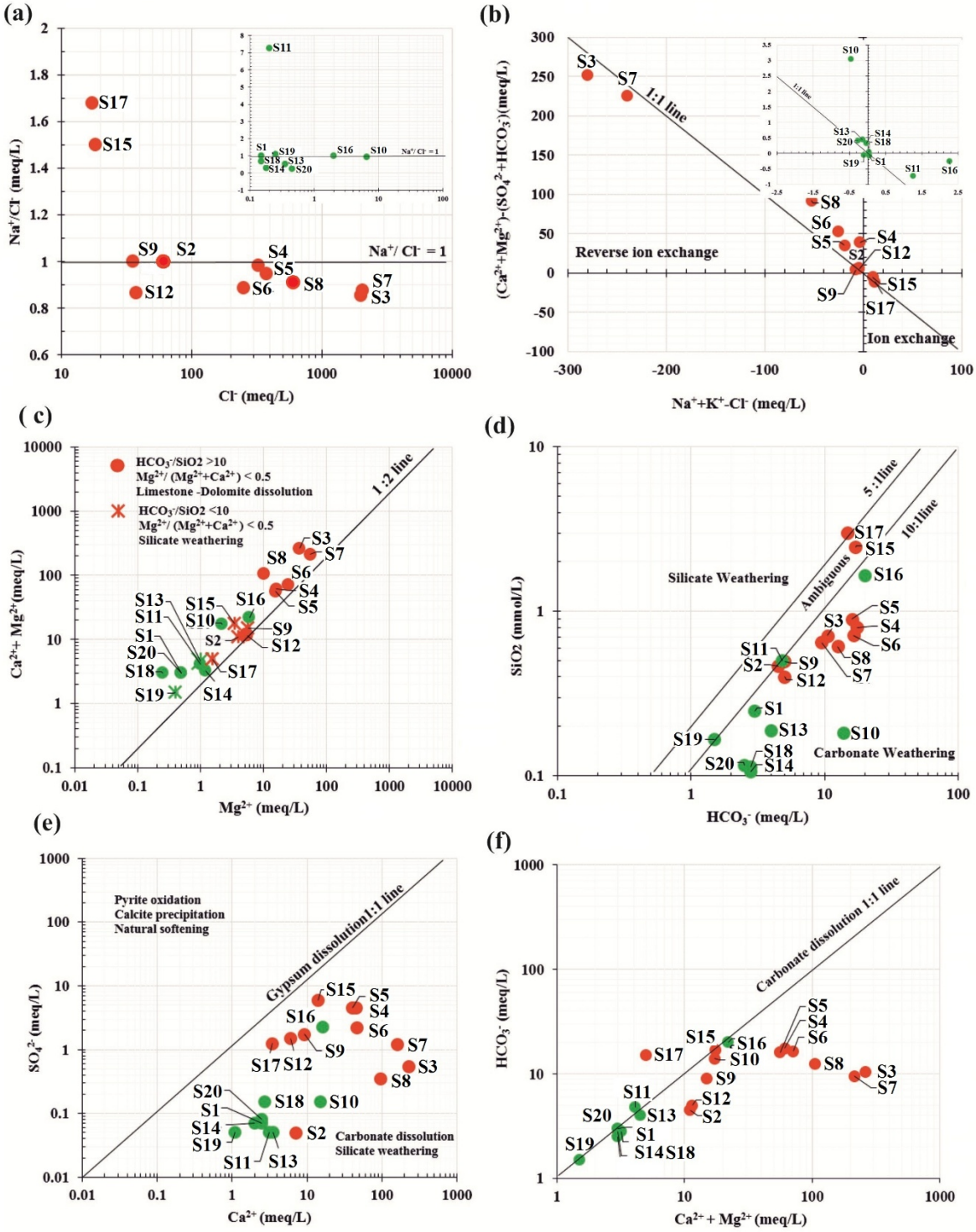

Fig. 2. Diagrams used to recognize hydrogeochemical processes based on the concentrations of major constituents in the spring waters. (a) Na^+ vs Cl^-, (b) $(Ca^{2+} + Mg^{2+})$ - $(HCO_3^- + SO_4^{2-})$ vs $(Na^+ + K^+ - Cl^-)$, (c) $(Ca^{2+} + Mg^{2+})$ vs Mg^{2+}, (d) SiO_2 vs HCO_3^-, (e) SO_4^{2-} vs Ca^{2+}, (f) HCO_3^- vs $(Ca^{2+} + Mg^{2+})$. The relations

for the a, c, d, e, and f diagrams were taken from Hounslow (2018), for the b diagram from Jalali (2005) (red and green circles represent Na-Cl thermal and Ca-HCO_3 non-thermal springs, respectively).

As displayed in Fig. 2b, among all the springs, S3, S7, and S17 thermal springs plot along a line with a gradient of -1 on $(Ca^{2+} + Mg^{2+}) - (SO_4^{2-} + HCO_3^-)$ versus $(Na^+ + K^+ - Cl^-)$. Sodium in S3 and S7 springs may get adsorbed and in S17 may get desorbed by underground clay layers during reverse ion exchange and ion exchange processes, respectively (Jankowski et al. 1998). The slightly higher ratio of Na^+/Cl^- in S2, S9, and S19 and considerably higher ratio of Na^+/Cl^- in S11, S15, and S17 suggest that high excess values of Na^+ is due to the weathering of granite-forming silicate minerals (Fig. 1) (Hounslow 2018, Woitischek et al. 2017). The weathering can also be applied to verify the $(Ca^{2+} + Mg^{2+})/Mg^{2+}$ and HCO_3^-/SiO_2 ratios. Considering Fig. 2c and d, HCO_3^- concentrations are lower than those of SiO_2 (< 10:1) and Mg^{2+} concentrations are lower than those of Mg^++Ca^{2+} concentrations (<0.5), probably reflecting silicate weathering (Morales-Arredondo et al. 2018).

All springs considered in this study are undersaturated with respect to gypsum and anhydrite (Table S2). The SO_4^{2-}/Ca^{2+} (in meq/L) ratio varied from 0.002 to 0.43 with a median of 0.10 in the thermal springs and from 0.01 to 0.14 with a median of 0.03 in non-thermal springs. In Fig. 2e, all samples plot below the gypsum dissolution line; meaning that the concentrations of Ca^{2+} are higher than SO_4^{2-}, which is likely be due to the dissolution of calcareous formations. Almost all the springs are either oversaturated or saturated with respect to calcite, aragonite, and dolomite (Table S2). The $(HCO_3^-)/(Ca^{2+} + Mg^{2+})$ (in meq/L) ratio of the samples varied from 0.04 to 3.03 with median of 0.29 in the thermal springs and from 0.81 to 1.17 with a median of 0.91 in the non-thermal springs. In this study, most thermal springs plot below the 1:1 line (Fig. 2f), indicating that the dissolution of dolomite is not the mere source of Ca^{2+}, Mg^{2+}, and HCO_3^- (Yuan et al. 2017).

4.3. Distribution of trace and radioactive elements

Descriptive statistics of As, Fe, U, and ^{226}Ra values in springs water samples is presented in Table 1. Arsenic varied from <LOD to 165 µg/L with a median of 1.50 µg/L in the thermal springs and 0.08 to 475 µg/L with a median of 0.45 µg/L in the non-thermal springs. High concentrations of As were detected in S15 and S17 thermal and S16 non-thermal springs (Fig. 3a). In hydrothermal fluids, As commonly occurs in inorganic forms including As oxyanions, neutral species, and thioarsenates/thioarsenites; however, methylated As compounds may also form under anoxic conditions (Bundschuh and Maity 2015).

Arsenic is generally enriched in Na-Cl type thermal fluids (Villanueva-Estrada et al. 2013). The associations between As and Cl^- is related to the similar behavior of these elements during subsurface boiling and phase separation (Centeno et al. 2016). Arsenic concentration in S16 is probably the result of mixing with As-rich thermal fluids or dissolution of As-rich carbonates. Iron concentration in the thermal springs varied from <LOD to 95 µg/L with a median of 8 µg/L and varied from 20 to 45 µg/L with a median of 35 µg/L in the non-thermal springs. The highest Fe concentrations was measured in S15 and S17 thermal springs (Fig. 3b). As shown in Fig. 2d, e, and f, the hydrochemistry of these springs seems to be affected by silicate weathering and carbonates dissolution. Uranium content in the thermal springs varied from <LOD to 0.90 µg/L with a median of 0.06 µg/L and from <LOD to 4.02 µg/L with a median of 0.74 µg/L

for the non-thermal springs. The highest U was measured in S11 and S19 non-thermal springs affected by silicate weathering (Fig. 2c and d, and 3c).

The U behavior in groundwater relies on redox conditions. Its main ions are U^{6+} under oxidizing conditions and U^{4+} under reducing condition. Concentration of U^{4+} is quite low as uranium concentration is commonly by the precipitation of low solubility uranium minerals such as $UO_{2\ (am)}$. In contrast, high concentrations of U^{6+} as UO_2^{2+} and/or $(UO_2)_2(CO_3)_2^{2-}$ may be present in carbonate/bicarbonate-rich oxidizing groundwater associated with granitic rocks weathering. U concentrations in the thermal springs were lower than the non-thermal springs probably due to low Eh of thermal springs water (Lauria 2004; Thivya et al. 2016).

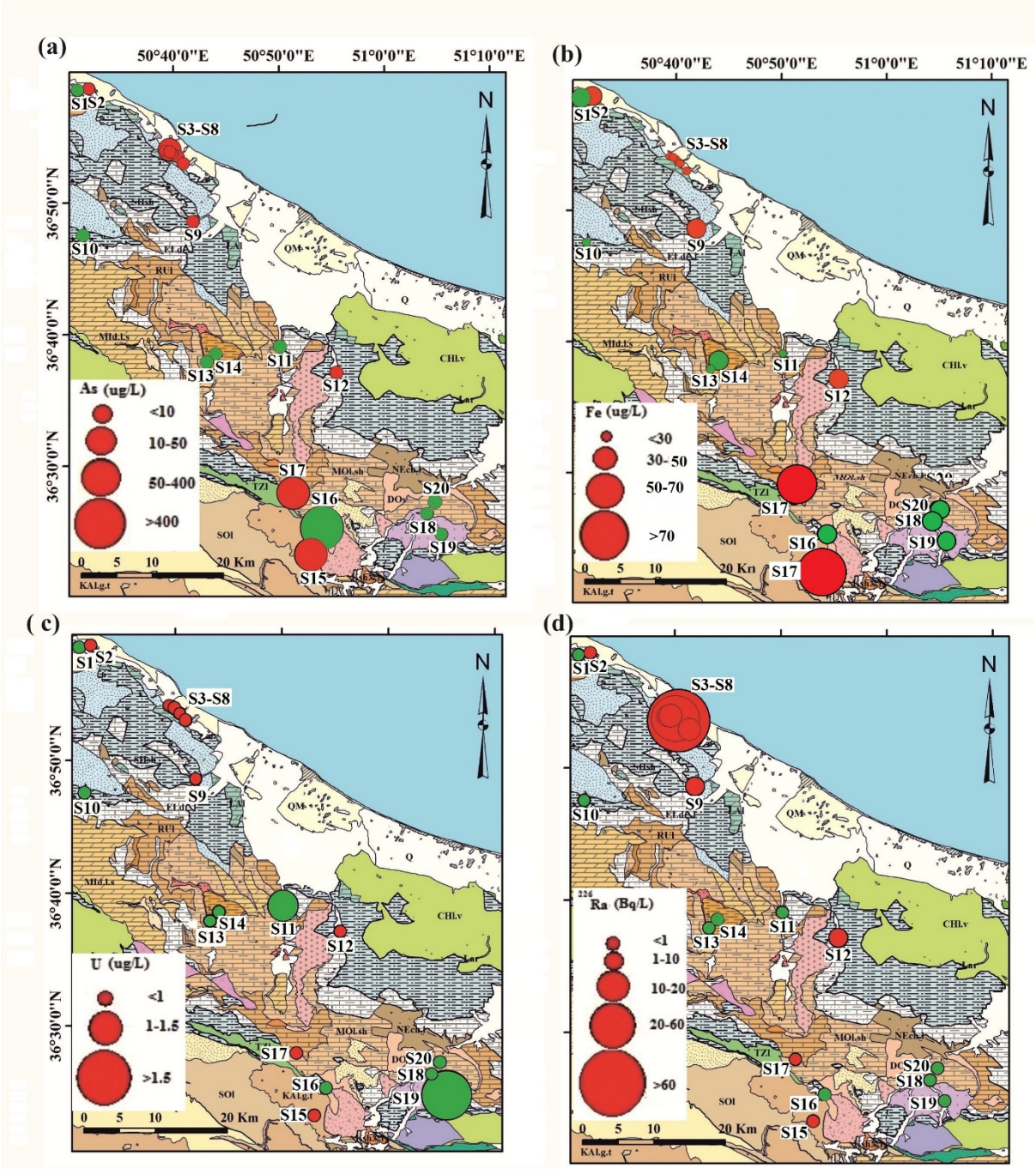

Fig. 3. Spatial distribution of (a) As, (b) Fe, (c) U, and (d) ^{226}Ra in the study area (red and green circles represent Na-Cl thermal and Ca-HCO_3 non-thermal springs, respectively).

Radium activity concentration in the thermal springs varied from <LOD to 64 Bq/L with a median of 1.50 Bq/L and in the non-thermal springs ranged from <LOD to 0.50 Bq/L with a median of 0.25 Bq/L. In fresh water, Ra tends to get rapidly adsorbed on aquifer solid phases, and hence its mobility is quite limited (Kraemer and Reid 1984). However, in hydrothermal fluids with low pH and Eh, and high temperature, Cl^- content and TDS, the activity concentration of ^{226}Ra is high (Zukin et al. 1987). Similar conditions were observed in Ramsar's thermal springs (Fig. 3d and Table S1). As shown in Fig. 3, distributions of As, Fe,

and ^{226}Ra vary in thermal springs. High concentrations of ^{226}Ra were encountered in north while high values of As and Fe occur spotted in south of the study area.

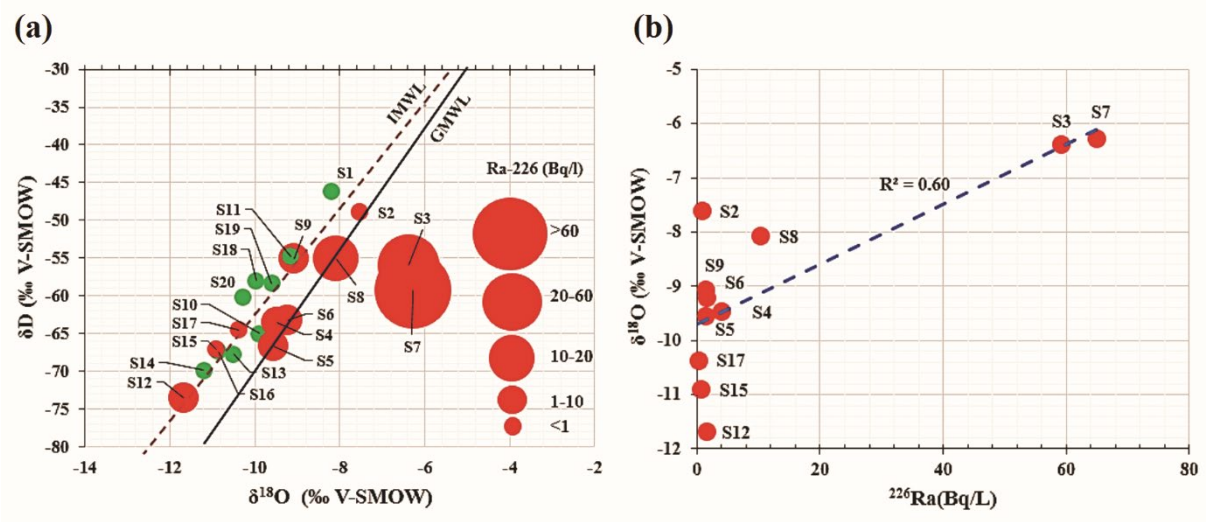

Fig. 4. Plots of (a) ^{226}Ra bubble diagram on δD vs $\delta^{18}O$ and (b) ^{226}Ra vs $\delta^{18}O$ of springs water (red and green circles represent Na-Cl thermal and Ca-HCO_3 non-thermal springs, respectively).

4.4. Isotopic chemistry of springs water

Stable isotope signature of the springs are commonly used to define the recharge origin of springs (Chatterjee et al. 2017: Sherif et al. 2018: Woitischek et al. 2017). The $\delta^{18}O$ values ranged from -11.68 to -6.29 ‰ (V-SMOW) for the thermal springs and -11.20 to -8.20 ‰ (V-SMOW) for the non-thermal springs. Moreover, δD values ranged from -73.56 to -48.97 ‰ for the thermal springs and -69.86 to -46.18 ‰ for the non-thermal springs. $\delta^{18}O$ versus δD plot is displayed in Fig. 4a. Iranian meteoric water line (IMWL, $\delta D=6.89\ \delta^{18}O+6.57$) (Shamsi and Kazemi 2014) and global meteoric water line (GMWL, $\delta D=8\ \delta^{18}O+10$) (Rozanski et al. 1993) are also plotted in Fig. 4a. All thermal springs, except S9, S12, S15, and S17, deviate from the IMWL indicating isotopic heavier signatures of the water, presumably effected by oxygen isotopic exchange during water-rock interaction (Chatterjee et al. 2017: Sherif et al. 2018: Woitischek et al. 2017). However, being thermal should not be considered a precondition for water-rock interaction. S9, S12, S15, and S17 thermal springs plotted on the IMWL, probably due to significant mixing with cold meteoric water (Pasvanoğlu 2013). Most of the non-thermal springs plot near the IMWL, indicating their meteoric origins (Li et al. 2018; Santaloia et al. 2016). The springs water with high ^{226}Ra (S3 and S7) displayed much higher $\delta^{18}O$ than the low ^{226}Ra springs water samples. The highest values occur in Ramsar's thermal springs (Fig. 4b).

4.5. Thermal springs classification

Ternary diagrams of Cl-SO_4-HCO_3 and Cl-Li-B were used to distinguish different types of hydrothermal systems on the basis of the major ions (Giggenbach 1988). As already pointed out, the results displayed two separate hydrothermal systems in the study area based on location and chemical composition. The north system include springs S2, S3, S4, S5, S6, S7, S8, S9, and S12 while the south system include S15 and S17 (Fig. 5a). Thermal springs of the north system with relatively high ^{226}Ra content fall in the Cl-rich region.

These springs are mature and probably formed by the interaction of thermal fluids with the host rock (Chenaker et al. 2018). In contrast, the springs in the south fall in the peripheral region specified by higher values of HCO_3^- than SO_4^{2-} and Cl^-, suggesting southern springs mixing with meteoric water enriched in HCO_3^- (Hernández-Morales and Wurl 2017). Based on Cl-Li-B ternary diagram, thermal springs plot towards the Cl-corner (Fig. 5b), indicating high Cl concentration relative to B and Li. The concentration of Cl^- in the northern system proved to be higher than the southern system probably as a result of thermal fluids mixing with secondary brines.

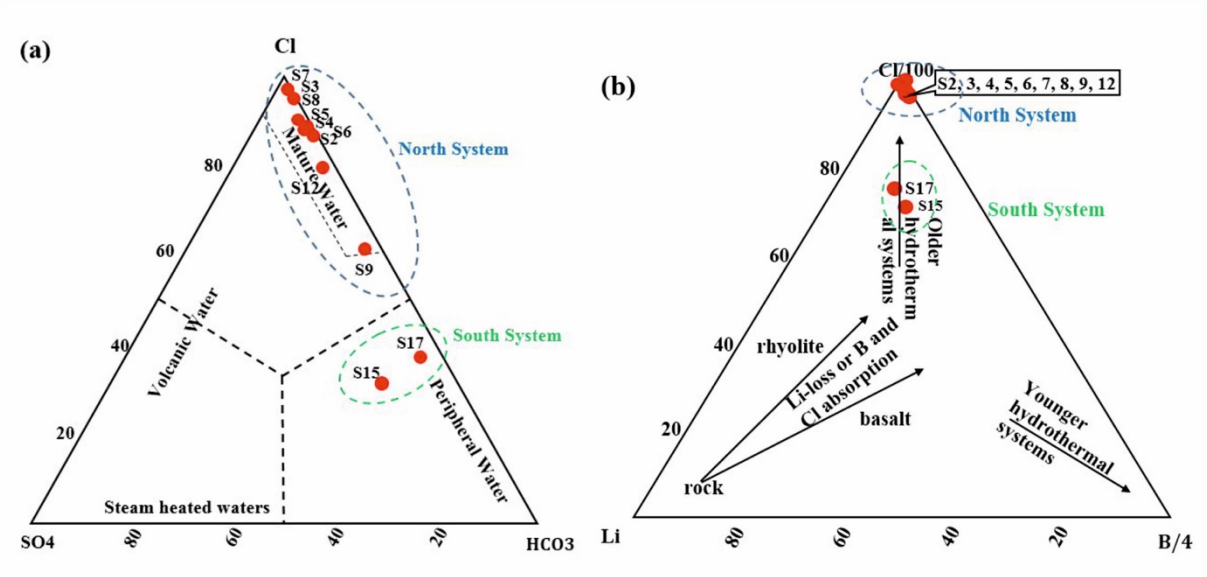

Fig. 5. (a) Giggenbach Cl-SO_4-HCO_3 and (b) Cl-Li-B ternary diagram of thermal springs (Giggenbach 1988).

4.6. Trace alkali metals (Li, Cs, and Rb) in thermal springs

Boron is a highly mobile and incompatible element during water–rock interaction process. Thus, boron is applied as a reference element for recognizing rock leaching in thermal springs water system (Schmidt et al. 2011). This is due to its high water/rock ratios, and inadequate clay minerals that may adsorb B, and its incorporation into the steam. Li, Cs, and Rb are less mobile than B. Therefore, B is probably preferentially released over trace alkali metals during rock leaching process (Kaasalainen et al. 2015). Trace alkali metals do not form their own hydrothermal minerals, but various prevalent secondary minerals including; quartz, feldspars, zeolites, and clays are known to scavenge them where these elements' replacement for K in the case of Rb and Cs, but probably Mg in the case of Li (Ollila et al. 2014). In this study, the relationship between the trace alkali metals (Li, Cs, and Rb) and B and K, as well as median rock ratios of rhyolite and basalt were investigated to understand the subsurface geochemical processes. The relations between Li, Cs, and Rb with B (Fig. 6a, b, and c) displays that most thermal springs plot below the rock ratios line meaning that the springs are depleted in Li, Cs, and Rb relative to their basaltic and rhyolitic ratios. This proposes either the release of B during rock leaching and/or uptake of metals into secondary minerals. Fig. S2 shows that the depletions are probably in part, due to both reasons (Kaasalainen and Stefánsson 2012; Wrage et al. 2017). When trace alkali metals were plotted against K (Fig. 6d, e, and

f), thermal springs matched those of the associated primary rocks primary rocks, indicating that these alkalis behave like K during water–rock interactions in the study area (Kaasalainen et al. 2015).

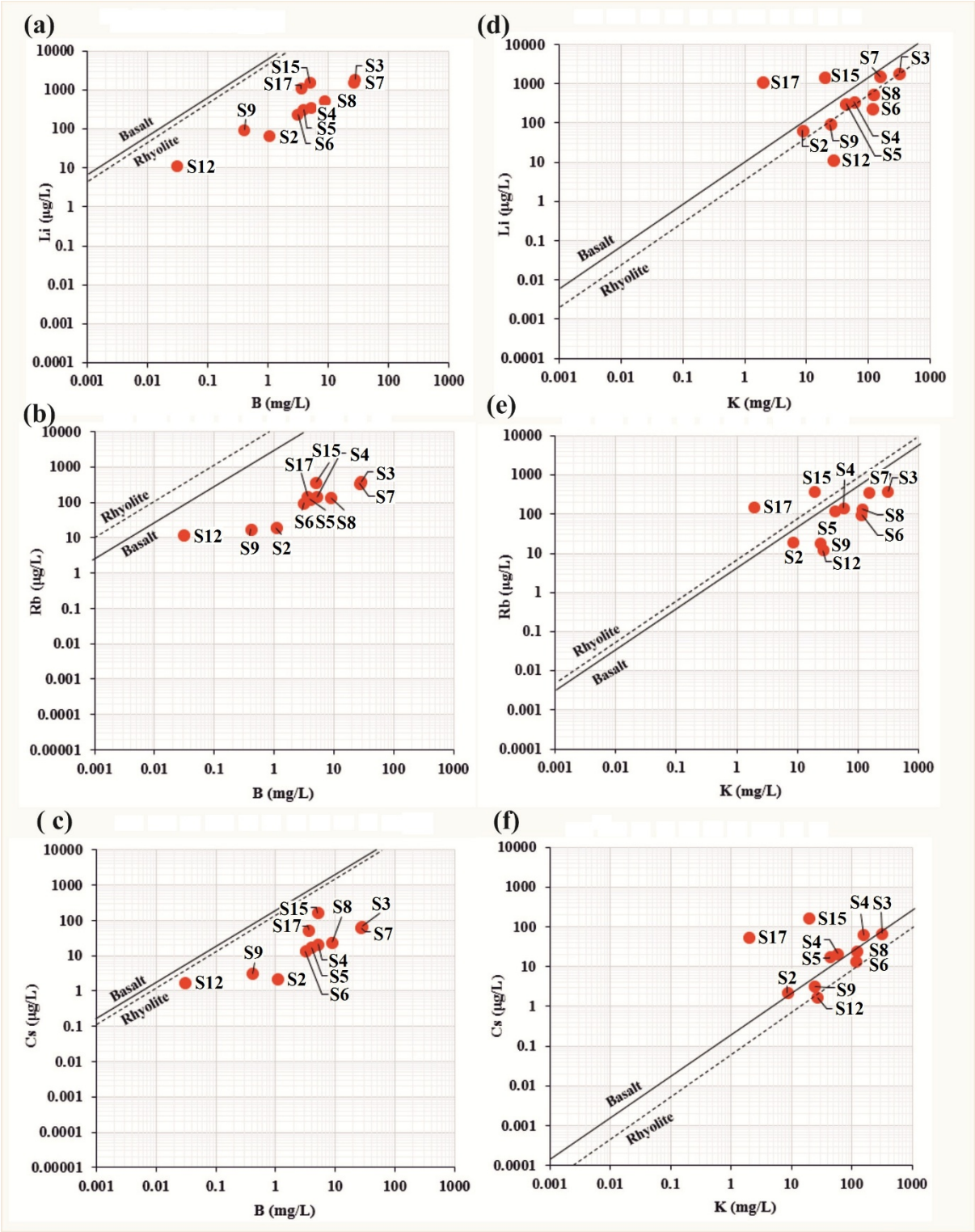

Fig. 6. Relationships between Li, Rb, and Cs vs B (a, b, and c) and K (d, e, and f) in thermal springs. Also shown are the median rock ratios of basalt (solid line) and rhyolite (dashed line). Graphs modified from Kaasalainen and Stefansson (Kaasalainen and Stefánsson 2012), with the median rock ratios as given by the authors and references therein.

Contrary to the north system springs, thermal springs of the south system plot higher above initial rock ratios (Fig. 6d, e, and f), suggesting enrichment in Li, Cs, and Rb relative to K (Kaasalainen and Stefánsson 2012). The reason is probably the fact that Li is highly soluble and does not remarkably participate in secondary minerals. On the other hand, although Cs may be incorporated into zeolites structure, its size is too large to replace other alkali metals in secondary minerals (Goguel 1983). Rubidium has a slightly larger ionic radius compared to K and enrichment in Rb over K is in compliance with the existence of Rb in zeolites, adularia, and clays (Kaasalainen and Stefánsson 2012). The geochemistry of trace alkali metals illustrated the role of rock leaching on the composition of thermal springs, in the study area.

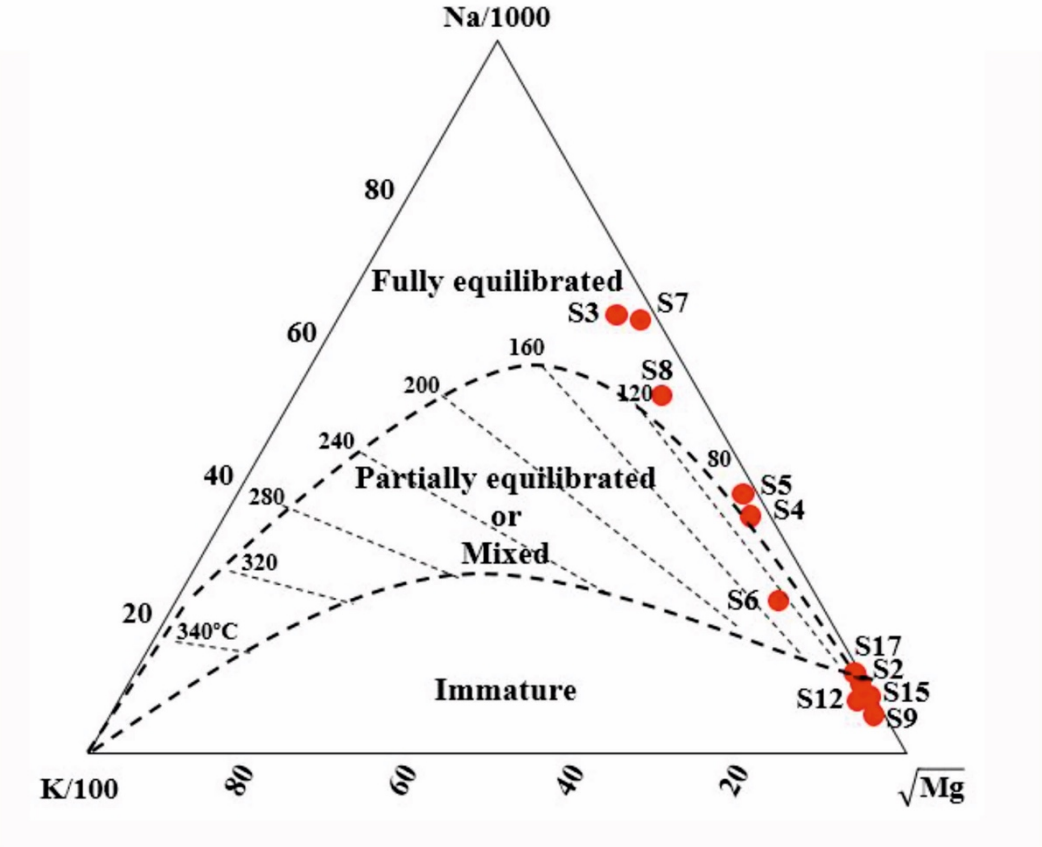

Fig. 7. Na-K-Mg ternary diagram of thermal springs in the study area (Giggenbach 1988).

4.7. Geothermometry

Solute geothermometers are commonly be used to estimate the water–rock equilibrium temperatures reached in subsurface hydrothermal reservoir (Anees et al. 2015). The Na-K-Mg ternary diagram merges the Na-K geothermometer with the K-Mg geothermometer to categorize thermal waters and conclude subsurface reservoir temperature according to the condition of equilibrium at given temperatures (Giggenbach 1988). In this study, some north thermal springs including S3, S5, S7, and S8 fall within the full equilibrium field, S4 and S6 plot within the partial equilibrium field, and the rest fall within the immature field (Fig. 7). Fully equilibrated water displays that the minerals in the water have probably

reached a fluid-rock equilibrium state. Partially equilibrated thermal water shows that minerals have been dissolved and equilibrium reactions have been set in, but equilibrium has not been attained. Partially equilibrated water result from mixing of equilibrated thermal water with a dilute unequilibrated water, such as cold groundwater. Immature water suggests the effects of several processes including re-equilibrium and strong dilution/mixing with shallow cold water (Giggenbach 1988).

The Na-K-Mg ternary diagram showed that temperature for all thermal springs is maximal around 140°C. Furthermore, in this study, quartz, chalcedony, Na-K, Na-K-Ca, and Na-Li geothermometers were applied to estimate the subsurface temperature of equilibrated and partially equilibrated thermal springs. These geothermometers comprises equations and temperature-dependent chemical reactions between water and minerals taking place in the hydrothermal reservoirs (Mukherjee 2012) (Table 2). Na-K-Ca geothermometer gave maximum reservoir temperatures (84-133°C), whereas Na-Li geothermometer gave the lowest temperatures (33-38°C).

Table 2. Estimation of the thermal reservoir temperature (°C) by different geothermometers (all units are in mg/L).

Spring	T °C	Quartz		Chalcedony		Na-K[e]	Na-K[f]	Na-K[g]	Na-K-Ca[h]	Na-Li[i]
		(maximum steam loss)[a]	(no loss of steam)[b]	(maximum steam loss)[c]	(no loss of steam)[d]					
S3	26.4	96	95	70	64	71	88	80	97	38
S4	48	101	100	75	70	71	88	80	96	38
S5	39.4	106	105	80	76	54	72	62	84	33
S6	39.6	96	95	71	64	122	137	136	133	38
S7	24.3	93	90	67	60	45	63	51	84	33
S8	32.4	91	88	65	57	79	96	88	105	35
Mean		97	96	71	65	74	91	83	100	36

[a] $T=\{1522/[5.75-\text{Log}(SiO_2)]\}-273.15$ (Fournier 1977)
[b] $T=\{1309/[5.19-\text{Log}(SiO_2)]\}-273.15$ (Fournier 1977)
[c] $T=\{1264/[5.31-\text{Log}(SiO_2)]\}-273.15$ (Fournier 1977)
[d] $T=\{1032/[4.96-\text{Log}(SiO_2)]\}-273.15$ (Fournier 1977)
[e] $T=\{1217/[1.438+\text{Log}(Na/K)]\}-273.15$ (Fournier 1979)
[f] $T=\{1390/[\text{Log}(Na/K)+1.750]\}-273.15$ (Giggenbach 1988)
[g] $T=\{1178/[\text{Log}(Na/K)+1.2393]\}-273.15$ (Nieva and Nieva 1987)
[h] $T=\{1647/[\text{Log}(Na/K)+\beta(\log(\sqrt{Ca}/Na)+2.06)+2.47]\}-273.15 \rightarrow \beta=4/3$ if $T<100$ °C, $\beta=1/3$ if $T>100$ °C (Fournier and Truesdell 1973)
[i] $T=\{1590/[\text{Log}(\text{Log}(Na/Li)+0.779]\}-273.15$ (Kharaka *et al.* 1982)

The Na-Li geothermometer presented significantly lower results. It does not seem to yield acceptable reservoir temperatures, because the calculated temperatures are lower than the water discharge temperature. This can be attributed to the relatively rapid exchange reactions of Li with clay minerals (Chenaker et al. 2018) or the influence of hydrothermal water-rock interactions on the thermal springs water chemistry (Saou et al. 2012). Reservoir temperatures obtained from maximum steam loss quartz geothermometer (91-106 °C) were similar to no steam loss quartz geothermometer (88-105 °C). This result probably is due to re-condensation of the steam during the ascent of thermal water (Chatterjee et al. 2017). Chalcedony geothermometer generally display lower temperature values compared to quartz geothermometer. It has been noted that quartz controls the dissolved SiO_2 content of thermal springs waters (Saxena and Gupta

1985). Therefore, regardless of the results of the Na-Li and chalcedony geothermometers, the average subsurface temperatures of ^{226}Ra source reservoir ranged from 83- 100°C.

4.8. Mechanisms controlling ^{226}Ra concentration in thermal springs

The concentration of ^{226}Ra in springs water is a function of several factors including parent isotope contents, rock leaching, Eh, pH, TDS, temperature, salinity, competing ion effects, adsorption/desorption on oxyhydroxides or organic matter, cation exchange mechanism and co-precipitation/dissolution processes (Dickson 1990; Sherif et al. 2018; Sturchio et al. 2001; Vinson et al. 2009). The geochemistry of trace alkali metals illustrated the occurrence of rock leaching in the study area. U content as a parent element of ^{226}Ra, is low in the thermal springs, while the elevated ^{226}Ra activity concentration is associated with reducing condition (Labidi et al. 2010; Vinson et al. 2009). Although Ra is not a redox-sensitive element, Fe and Mn oxyhydroxides, which are responsible for Ra adsorption, are sensitive to reductive dissolution in aqueous systems.

The lack of dissolved oxygen creates thermodynamically unstable conditions for solid-phase metal oxides which remove Ra from water (Vinson et al. 2013). On the other hand, as seen in Fig. 8a, ^{226}Ra showed a week negative correlation with pH (R^2= -0.40) because of the increasing surface charge of possible Ra^{2+}-adsorbing minerals as pH decreases (Vinson et al. 2013). The plot of ^{226}Ra against TDS is presented in Fig. 8b. In this case the correlation coefficient is significantly positive (R^2=0.96) indicating that high values of TDS can prevent the adsorption of Ra on aquifer adsorbents due to (1) the competition of alkaline-earth metals cations with Ra for the adsorption sites (Lauria et al. 2004; Szabo et al. 2005; Vinson et al. 2009, 2013); (2) the increase in the charge of mineral surface (Sturchio et al. 2001); (3) the increase in the stability of radium inorganic complexes (Hammond et al. 1988), and (4) the formation of strong organic complexes in high-ionic-strength solutions (Dickson 1990).

Radium may not be involved in clay minerals cation exchange reactions which has been identified as a mechanism that may significantly limit ^{226}Ra concentration in groundwater (Oden and Szabo 2016; Stackelberg et al. 2018). Radium showed a positive linear relationship with Cl (R^2=0.55) (Fig. 8c). This can be explained by the fact that Ra is more mobile in higher Cl water (Labidi et al. 2010; Souza et al. 2010). The resemblance of Ra^{2+} and other divalent alkaline-earth cations ionic radii and polarizability illustrates a tendency for Ra^{2+} to co-precipitate with these elements in mineral lattices (Rosenberg et al. 2011; Sherif et al. 2018). In the study area, springs water Ra showed positive correlations with Ba (R^2= 0.94) and Ca (R^2= 0.85) (Fig. 8d and e) implying that the existence of Ba and Ca are connected to ^{226}Ra removal via co-precipitation of Ba- sulfates (Curti et al. 2010; Vinson et al. 2013) and Ca-carbonates (Gnanapragasam and Lewis 1995; Grandia et al. 2008).

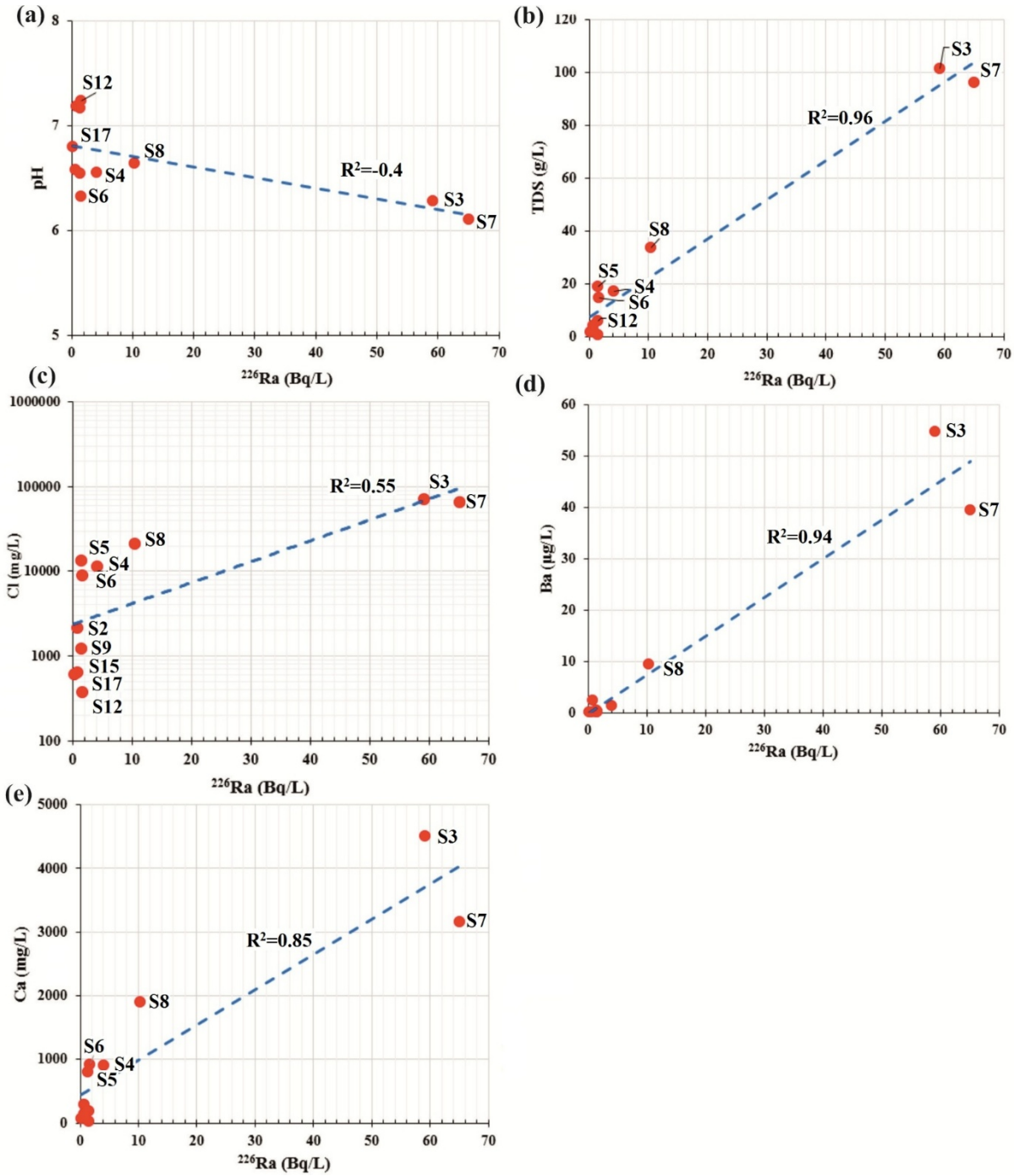

Fig. 8. Relationships between Ra vs (a) pH, (b) TDS, (c) Cl, (d) Ba, and (e) Ca in thermal springs

5. Conclusion

Elevated ^{226}Ra activity concentrations in the Ramsar area were measured in Na-Cl thermal springs where water is generally characterized with low pH and Eh, high temperature, Cl^- content and TDS and positive shift related to $\delta^{18}O$. Highest concentrations of As, Li, Cs, Rb, Sr, Ba, B, Br^-, F^-, NO_3^-, PO_4^{3-} and SiO_2 were also measured in thermal springs. The low Br/Cl and Na^+/Cl^- molar ratios along with a positive correlation between Cl^- and $\delta^{18}O$ is suggestive of the influence of hydrothermal fluids on ^{226}Ra rich thermal

springs. Cl-SO_4-HCO_3 and Cl-Li-B ternary diagrams confirmed that Ramsar thermal springs can be categorized as old hydrothermal fluids with low magmatic degassing. On the other hand, the geochemistry of trace alkali metals illustrated the influence of rock leaching on the composition of thermal springs. Moreover, the hydrochemical composition of thermal springs provides evidence that their ^{226}Ra is sourced mainly from the decay of parent nuclides in connection with hydrothermal fluids and high temperature water-rock interactions. Since thermal springs are supersaturated or saturated with respect to barite and calcite, ^{226}Ra may be removed from water through co-precipitation processes. Nevertheless, the authors suggest a detailed investigation on the petrography, whole-rock geochemistry, and mineral chemistry of surrounding geological formations to reveal possible influences on the hydrochemistry of springs.

Acknowledgements

The authors of this paper would like to express their gratitude to Radiation Research Center of Shiraz University and Nuclear Science and Technology Research Institute for financial and logistic supports.

Reference

Alavi M (1996) Tectonostratigraphic synthesis and structural style of the Alborz Mountain System in Northern Iran. J Geodyn 21(1): 1–33.

Alçiçek H, Bülbül A, Alçiçek MC (2016) Hydrogeochemistry of the thermal waters from the Yenice geothermal field (Denizli Basin, Southwestern Anatolia, Turkey. J Volcanol Geotherm Res 309: 118-138.

Amini Birami F, Moore F, Faghihi R, Keshavarzi B (2019) Distribution of natural radionuclides and assessment of the associated radiological hazards in the rock and soil samples from a high-level natural radiation area, Northern Iran. J Radioanal Nucl Ch 322(3): 2091-2103.

Amini Birami F, Moore F, Faghihi R, Keshavarz, B (2020) Assessment of spring water quality and associated health risks in a high-level natural radiation area, North Iran. Environ Sci Pollut Res 1-14.

Anees M, Shah MM, Qureshi AA (2015) Isotope studies and chemical investigations of Tattapani hot springs in Kotli (Kashmir, NE Pakistan): implications on reservoir origin and temperature. Procedia Earth Planet Sci 13: 291-295.

APHA (1995) Standard methods for the examination of water and wastewater, 19th Ed, American Public Health Association.

ASTM (2004) Standard practices for the measurement of radioactivity (D3648), Vol. 11.02.

Belhai M, Fujimitsu Y, Bouchareb-Haouchine FZ, Iwanaga, T, Noto M, Nishijima J (2016) Hydrogeochemical and isotope geochemical study of northwestern Algerian thermal waters. Arab J Geosci 9(3): 169.

Berberian F, Muir ID, Pankhurst RJ, Berberian M (1982) Late Cretaceous and Early Miocene Andean-type plutonic activity in northern Makran and Central Iran. J Geolo Soc Lond 139, 605-614.

Bozkurt A, Yorulmaz N, Kam E, Karahan G, Osmanlioglu AE (2007) Assessment of environmental radioactivity for Sanliurfa region of southeastern Turkey. Radiat Meas 42(8): 1387-1391.

Bundschuh J, Maity JP (2015) Geothermal arsenic: occurrence, mobility and environmental implications. Renew Sustain Energy Rev 42: 1214-1222.

Cartier EG (1971) Geology of the lower Chalus Valley, central Alborz, Iran. Geological institute, ETH-Zurich, pp. 1–164.

Centeno J, Finkelman R, Selinus O (2016) Medical geology: Impacts of the natural environment on public health.

Chatterjee S, Sarkar A, Deodhar AS, Biswal BP, Jaryal A, Mohokar HV, Dash A (2017) Geochemical and isotope hydrological characterization of geothermal resources at Godavari valley, India. Environ Earth Sci 76(2): 97.

Chenaker H, Houha B, Vincent V (2018) Hydrogeochemistry and geothermometry of thermal water from north-eastern Algeria. Geothermics 75: 137-145.

Curti E, Fujiwara K, Iijima K, Tits J, Cuesta C, Kitamura A, Müller W (2010) Radium uptake during barite recrystallization at 23±2° C as a function of solution composition: An experimental ^{133}Ba and ^{226}Ra tracer study. Geochim Cosmochim Acta. 74(12): 3553-3570.

Dickson BL (1990) Radium in groundwater. The environmental behavior of radon, Ch. 4-2. IAEA Technical Report Series 310: 335–371.

Fathabadi N, Salehi AA, Naddafi K, Kardan M.R, Yunesian M, Nodehi RN, Karimi M (2017) Radioactivity levels in the mostly local foodstuff consumed by residents of the high level natural radiation areas of Ramsar, Iran. J Environ Radioact 169: 209-213.

Fathabadi N, Salehi AA, Naddafi K, Kardan MR, Yunesian M, Nodehi RN, Shooshtari MG (2019) Public ingestion exposure to 226Ra in Ramsar, Iran. J Environ Radioact 198, 11-17.

Fournier RO (1979) A revised equation for the Na/K geothermometer. Transactions of the Geothermal Resources Council 3: 221-224.

Fournier RO (1977) Chemical geothermometers and mixing models for geothermal systems. Geothermics 5(1-4): 41–50.

Fournier RO, Truesdell AH (1973) An empirical Na-K-Ca geothermometer for natural waters. Geochim Cosmochim Acta 37(5): 1255–1275.

Ghiassi-Nejad M, Mortazavi SMJ, Cameron JR, Niroomand-Rad A, Karam PA (2002) Very high background radiation areas of Ramsar, Iran: preliminary biological studies. Health Phys 82(1): 87-93.

Giggenbach WF (1988) Geothermal solute equilibria, derivation of Na-K-Mg-Ca geoindicators. Geochimica et Cosmochimica Acta 52(12): 2749-2765.

Giggenbach WF (1991) Chemical techniques in geothermal exploration. Application of geochemistry in geothermal reservoir development 119-144.

Gnanapragasam EK, Lewis BAG (1995) Elastic strain energy and the distribution coefficient of radium in solid solutions with calcium salts. Geochim Cosmochim Acta 59(24): 5103-5111.

Goguel R (1983) The rare alkalies in hydrothermal alteration at Wairakei and Broadlands, geothermal fields, NZ. Geochim Cosmochim Acta 47(3): 429-437.

Grandia F, Merino J, Bruno J (2008) Assessment of the radium-barium co-precipitation and its potential influence on the solubility of Ra in the near-field (No. SKB-TR--08-07), Swedish Nuclear Fuel and Waste Management Co.

Guest B, Axen GJ, Lam PS, Hassanzadeh J (2006) Late Cenozoic shortening in the west-central Alborz Mountains, northern Iran, by combined conjugate strike-slip and thin-skinned deformation. Geosphere 2:35–52.

Hammond DE, Zukin JG, Ku TL (1988) The kinetics of radioisotope exchange between brine and rock in a geothermal system. J Geophys Res Sol Ea 93(B11): 13175-13186.

Hernández-Morales P, Wurl J (2017) Hydrogeochemical characterization of the thermal springs in northeastern of Los Cabos Block, Baja California Sur, México. Environ Sci Pollut Res 24(15): 13184-13202.

Hounslow A (2018) Water quality data: analysis and interpretation. CRC press.

Jalali M (2005) Major ion chemistry of groundwaters in the Bahar area, Hamadan, western Iran. Environ Geol 47(6): 763-772.

Jankowski J, Acworth R I, Shekarforoush S (1998) Reverse ion-exchange in deeply weathered porphyritic dacite fractured aquifer system, Yass. In New South Wales Australia. In: Arehart GB, Hulston JR (eds) Proceedings of 9th international symposium on water–rock interaction, Taupo, New Zealand (Vol. 30, pp. 243-246).

Kaasalainen H, Stefánsson A (2012) The chemistry of trace elements in surface geothermal waters and steam, Iceland Chem Geol 330: 60-85.

Kaasalainen H, Stefánsson A, Giroud N, Arnórsson S (2015) The geochemistry of trace elements in geothermal fluids, Iceland. Appl Geochem 62: 207-223.

Khademi B, Alemi AA, Nasseri A (1980) Transfer of radium from soil to plants in an area of high natural radioactivity in Ramsar, Iran. Natural radiation environment III. Volume I, 600-610.

Khademi B, Mesghali A (1971) Investigation and measurement of radium in Ramsar mineral water. Health Phys 21(3): 464-465.

Khademi B, Tahsili A (1972) Environmental radioactivity in certain parts of Iran (No. CONF-720805-P1).

Khademi B, Sekhavat A, Parnianpour H (1975) Area of natural background radiation in the northern part of Iran. In international symposium on areas of high natural radioactivity, Brasil (Vol. 186).

Khairy H, Janardhana MR, Etebari B (2013) Conceptualization of the hydrogeological system of southern Caspian Coastal Aquifer of Amol - Ghaemshahr Plain, Mazandaran Province, Iran. Int J Earth Sci Eng 6(5): 1222–1235.

Kharaka YK, Lico MS, Law LM (1982) Chemical geothermometers applied to formation waters, Gulf of Mexico and California basins. AAPG Bulletin 66(5): 588-588.

Kloppmann W, Négrel P, Casanova J, Klinge H, Schelkes K, Guerrot C (2001) Halite dissolution derived brines in the vicinity of a Permian salt dome (N German Basin). Evidence from boron, strontium, oxygen, and hydrogen isotopes. Geochim Cosmochim Acta 65(22): 4087-4101.

Knoll GF (2010) Radiation detection and measurement. John Wiley & Sons, Inc., New York.

Kraemer TF, Reid DF (1984) The occurrence and behavior of radium in saline formation water of the US Gulf Coast region. Chem Geol 46(2): 153-174.

Labidi S, Mahjoubi H, Essafi F, Salah, RB (2010) Natural radioactivity levels in mineral, therapeutic and spring waters in Tunisia. Radiat Phys Chem 79(12): 1196-1202.

Lauria DC, Almeida RMR, Sracek O (2004) Behavior of radium, thorium and uranium in groundwater near the Buena Lagoon in the Coastal Zone of the State of Rio de Janeiro, Brazil Environ Geol 47(1): 11-19.

Li Z, Wang G, Wang X, Wan L, Shi Z, Wanke H, Uahengo CI (2018) Groundwater quality and associated hydrogeochemical processes in Northwest Namibia. J Geochem Explor 186: 202-214.

Meinzer OE (1923) Outline of ground-water hydrology with definitions: US Geological Survey Water-Supply Paper 494, 71 p. 1927. Plants as indicators of ground water: US Geological Survey Water-Supply Paper. 577, 95.

Michel J (1990) Relationship of radium and radon with geological formations. Radon, radium and uranium in drinking water. 7: 83-95.

Miller RL, Sutcliffe H (1985) Occurrence of natural radium-226 radioactivity in ground water of Sarasota County, Florida (Vol. 84, No. 4237). US Geological Survey.

Morales-Arredondo JI, Esteller-Alberich MV, Hernández MA, Martínez-Florentino TAK (2018) Characterizing the hydrogeochemistry of two low-temperature thermal systems in Central Mexico. J Geochem Explor 185: 93-104.

Mukherjee S (2012) Applied mineralogy: applications in industry and environment. Springer Science & Business Media.

Nair RRK, Rajan B, Akiba S, Jayalekshmi P, Nair MK, Gangadharan P, Kog T, Morishima H, Nakamura S, Sugahara T(2009) Background radiation and cancer incidence in Kerala, India-Karanagappally cohort study. Health Phys 96(1): 55-66.

Nazari H, Shahidi A (2011) Tectonic of Iran, Alborz. Geological Survey and Mineral Exploration of Iran. Research Institute for Earth Science, p. 97.

Nieva D, Nieva R (1987) Developments in geothermal energy in Mexico—part twelve. A cationic geothermometer for prospecting of geothermal resources. Heat recovery systems and CHP. 7(3): 243-258.

Oden JH, Szabo Z (2016) Arsenic and radionuclide occurrence and relation to geochemistry in groundwater of the Gulf Coast Aquifer System in Houston, Texas, 2007–11 (No. 2015-5071). US Geological Survey.

Ollila AM, Newsom HE, Clark III B, Wiens RC, Cousin A, Blank JG, Gasnault O (2014) Trace element geochemistry (Li, Ba, Sr, and Rb) using Curiosity's ChemCam: early results for Gale crater from Bradbury landing site to Rocknest. J Geophys Res Planets 119(1): 255-285.

Parkhurst DL, Appelo CAJ (2013) Description of input and examples for PHREEQC version 3: a computer program for speciation, batch-reaction, one-dimensional transport, and inverse geochemical calculations (No. 6-A43). US Geological Survey.

Paschoa AS (2000) More than forty years of studies of natural radioactivity in Brazil. Technology. 7(2-3): 193-212.

Pasvanoğlu S (2013) Hydrogeochemistry of thermal and mineralized waters in the Diyadin (Ağri) area, Eastern Turkey. Appl Geochem 38: 70-81.

Pervov AG, Andrianov AP, Efremov RV, Desyatov AV, Baranov AE (2003) A new solution for the Caspian Sea desalination: low-pressure membranes. Desalination 157(1-3): 377-384.

Piper AM (1953) A graphic procedure for the geo-chemical interpretation of water analysis. USGS groundwater (No. 12). note.

Pirajno F (2013) Hydrothermal Processes and Mineral Systems. J Chem Inf Model 53(9): 1689–1699.

Qureshi AA, Tariq S, Din KU, Manzoor S, Calligaris C, Waheed A (2014) Evaluation of excessive lifetime cancer risk due to natural radioactivity in the rivers sediments of Northern Pakistan. J Radiat Res Appl Sci 7(4): 438-447.

Rosenberg YO, Metz V, Oren Y, Volkman Y, Ganor J (2011) Co-precipitation of radium in high ionic strength systems: 2. Kinetic and ionic strength effects. Geochim Cosmochim Acta 75(19): 5403-5422.

Rozanski K, Araguás-Araguás L, Gonfiantini R (1993) Isotopic patterns in modern global precipitation. Climate change in continental isotopic records 78: 1-36.

Santaloia F, Zuffianò LE, Palladino G, Limoni PP, Liotta D, Minissale A, Polemio M (2016) Coastal thermal springs in a foreland setting: The Santa Cesarea Terme system (Italy). Geothermics 64: 344-361.

Saou A, Maza M, Seidel JL (2012) Hydrogeochemical Processes Associated with Double Salinization of Water in an Algerian Aquifer, Carbonated and Evaporitic. Pol J Environ Stud 21(4): 1013–1024.

Saxena VK, Gupta ML (1985) Aquifer chemistry of thermal waters of the Godavari valley, India. J Volcanol Geotherm Res 25(1-2): 181-191.

Schmidt K, Garbe-Schönberg D, Koschinsky A, Strauss H, Jost CL, Klevenz V, Königer P (2011) Fluid elemental and stable isotope composition of the Nibelungen hydrothermal field (8 18′ S, Mid-Atlantic Ridge): Constraints on fluid–rock interaction in heterogeneous lithosphere. Chem Geol 280(1-2): 1-18.

Shamsi A, Kazemi G (2014) A review of research dealing with isotope hydrology in Iran and the first Iranian meteoric water line. Geopersia 4(1): 73-86.

Sheikhy Narany T, Ramli MF, Aris Zaharin A, Sulaiman WNA, Juahir H, Fakharian K (2014) Identification of the hydrogeochemical processes in groundwater using classic integrated geochemical methods and geostatistical techniques, in Amol-Babol plain, Iran. The Scientific World Journal, 2014.

Sherif MI, Lin J, Poghosyan A, Abouelmagd A, Sultan MI, Sturchio NC (2018) Geological and hydrogeochemical controls on radium isotopes in groundwater of the Sinai Peninsula, Egypt. Sci Total Environ 613: 877-885.

Shorabi M (1990) Recent Radiological Studies of High Level Natural Radiation Areas of Ramsar. Proceeding of international conference on high levels of natural radiation; Ramsar, Iran. Vienna: IAEA: 3–7.

Sohrabi M, Esmaili AR (2002) New public dose assessment of elevated natural radiation areas of Ramsar (Iran) for epidemiological studies. In International Congress Series. 1225, 15-24.

Sohrabi M (2013) World high background natural radiation areas: Need to protect public from radiation exposure. Radiat Meas 50: 166-171.

Sohrabi M, Babapouran M (2005) New public dose assessment from internal and external exposures in low-and elevated-level natural radiation areas of Ramsar, Iran. In International Congress Series. 1276: 169-174.

Souza TA, Godoy JM, Godoy MLD, Moreira I, Carvalho ZL, Salomão MSM, Rezende CE (2010) Use of multitracers for the study of water mixing in the Paraíba do Sul River estuary. J Environ Radioact 101(7): 564-570.

Stackelberg PE, Szabo Z, Jurgens BC (2018) Radium mobility and the age of groundwater in public-drinking-water supplies from the Cambrian-Ordovician aquifer system, north-central USA. Appl Geochem 89: 34-48.

Stampfli GM (2000) Tethyan oceans. In: Bozkurt, E., Winchester, J.A., Piper, J.D.A. (Eds.), Tectonics and Magmatism in Turkey and Surrounding Area, 173. Geological Society of London, Special Publication, pp. 163-185.

Sturchio NC, Banner JL, Binz CM, Heraty LB, Musgrove M (2001) Radium geochemistry of ground waters in Paleozoic carbonate aquifers, midcontinent, USA. Appl Geochem 16(1): 109-122.

Szabo Z, DePaul VT, Kraemer TF, Parsa B (2005) Occurrence of radium-224, radium-226, and radium-228 in water of the unconfined Kirkwood-Cohansey aquifer system, southern New Jersey. U. S. Geological Survey.

Tabar E, Kumru MN, Ichedef M ,Saç MM (2013) Radioactivity level and the measurement of soil gas radon concentration in Dikili geothermal area, Turkey. Int J Radiat Res 11(4): 253-261.

Tao Z, Akiba S, Zha Y, Sun Q, Zou j (2012) Cancer and non-cancer mortality among inhabitants in the high background radiation area of Yangjiang, China (1979–1998). Health Phys 102(2),: 173-181.

Thivya C, Chidambaram S, Keesari T, Prasanna MV, Thilagavathi R, Adithya VS, Singaraja C (2016) Lithological and hydrochemical controls on distribution and speciation of uranium in groundwaters of hard-rock granitic aquifers of Madurai District, Tamil Nadu (India). Environ Geochem Health 38(2): 497-509.

Todd D K, Mays LW (2005) Groundwater hydrology. 3rd edition. Welly Inte.

Tuzhilkin VS, Katunin DN, Nalbandov YR(2005) Natural chemistry of Caspian Sea waters. In The Caspian Sea Environment (pp. 83-108). Springer, Berlin, Heidelberg.

UNSCEAR (2000) Report Sources and Effects of Ionizing Radiation, United Nations Scientific Committee on the Effects of Atomic Radiation UNSCEAR 2000 Report to the General Assembly, with Scientific Annexes.

Vahdati Daneshmand F, Karimkhani A, Karimi H (2001) Geological map of Chalus (sheet 6263), scale 1:100000. Geological survey of Iran.

Vahdati Daneshmand F (2004) Geological map of Marzanabad (1/100000). Geological Survey of Iran, Tehran.

Vengosh A, De Lange GJ, Starinsky A (1998) Boron isotope and geochemical evidence for the origin of Urania and Bannock brines at the eastern Mediterranean: Effect of water-rock interactions. Geochim Cosmochim Acta 62(19-20): 3221-3228.

Villanueva-Estrada RE, Prol-Ledesma RM, Rodríguez-Díaz AA, Canet C, Armienta MA (2013) Arsenic in hot springs of Bahía Concepción, Baja California Peninsula, México. Chem Geol 348: 27-36.

Vinson DS, Tagma T, Bouchaou L, Dwyer GS, Warner NR, Vengosh A (2013) Occurrence and mobilization of radium in fresh to saline coastal groundwater inferred from geochemical and isotopic tracers (Sr, S, O, H, Ra, Rn). Appl Geochem 38: 161-175.

Vinson DS, Vengosh A, Hirschfeld D, Dwyer GS (2009) Relationships between radium and radon occurrence and hydrochemistry in fresh groundwater from fractured crystalline rocks, North Carolina (USA). Chem Geol 260(3-4): 159-171.

Woitischek J, Dietzel M, Inguaggiato C, Böttcher ME, Leis A, Cruz JV, Gehre M (2017) Characterisation and origin of hydrothermal waters at São Miguel (Azores) inferred by chemical and isotopic composition. J Volcanol Geotherm Res 346: 104-117.

Wrage J, Tardani D, Reich M, Daniele L, Arancibia G, Cembrano J, Pérez-Moreno R (2017) Geochemistry of thermal waters in the Southern Volcanic Zone, Chile–Implications for structural controls on geothermal fluid composition. Chem Geol 466: 545-561.

Yuan J, Xu F, Deng G, Tang Y, Li P (2017) Hydrogeochemistry of shallow groundwater in a karst aquifer system of Bijie city, Guizhou Province. Water 9(8): 625.

Zanchi A, Berra F, Mattei M, Ghassemi M, Sabouri J (2006) Inversion tectonics in central Alborz, Iran. J Struct Geol 28:2023–2037.

Zarei M, Raeisi E, Merkel BJ, Kummer NA (2013) Identifying sources of salinization using hydrochemical and isotopic techniques, Konarsiah, Iran. Environ Earth Sci 70(2): 587-604.

Zukin JG, Hammond DE, Teh-Lung K, Elders WA (1987) Uranium-thorium series radionuclides in brines and reservoir rocks from two deep geothermal boreholes in the Salton Sea Geothermal Field, southeastern California. Geochim Cosmochim Acta 51(10): 2719-2731.

Supplementary Materials

Table S1. Physicochemical parameters and chemical and isotopic composition of the spring water samples.

Sample	T	TDS	EC	Eh	pH	Ca^{2+}	Mg^{2+}	Na^{+}	K^{+}	HCO_3^{-}	Cl^{-}	SO_4^{2-}	Water type	Error
	°C	g/L	mS/cm	mV		meq/L								%
S1	14	0.25	0.32	300	7.35	2.50	0.50	0.15	0.04	3	0.15	0.07	Ca-HCO_3^{-}	0.46
S2	24	4	6.40	359	7.18	7	4	60.20	0.22	4.50	60	0.05	Na-Cl	-5.05
S3	26	103	187	68	6.28	225	37.50	1712	8.03	10.50	2000	0.55	Na-Cl	0.71
S4	48	17	27.33	10	6.55	45	16	320	1.50	17.50	325	4.50	Na-Cl	-4.87
S5	39	18.83	33.12	98	6.54	40.30	15.47	355	1.10	16	375	4.50	Na-Cl	-2.03
S6	40	14.54	26.41	87	6.32	46	25	222	3	16.50	250	2.25	Na-Cl	-4.83
S7	24	96.24	173	65	6.10	158	55	1800	4	9.50	2050	1.20	Na-Cl	1.07
S8	32	33.50	60.50	45	6.64	95	10	544.36	3.06	12.50	600	0.35	Na-Cl	-3.13
S9	26	0.42	4.86	359	7.17	9.20	5.60	35	0.62	9	35	1.75	Na-Cl	-4.84
S10	15	0.54	2	302	9.15	15	2.20	6	0.04	14	6.50	0.15	Ca-HCO_3^{-}	0.87
S11	14	0.31	3.38	280	7.68	3.12	1	1.45	0.01	4.80	0.20	0.05	Ca-HCO_3^{-}	-4.99
S12	35	0.87	1.65	90	7.24	6	5.50	32	0.7	5	37	1.50	Na-Cl	-0.80
S13	12	0.12	1.26	323	7.76	3.50	1	0.18	0.03	4	0.35	0.05	Ca-HCO_3^{-}	0.95
S14	16	0.15	0.47	285	8.42	2	1.20	0.05	0.10	2.80	0.18	0.07	Ca-HCO_3^{-}	-4.69
S15	37	2.30	4	368	6.58	14	3.50	27	0.50	17	18	6	Na-Cl	-4.65
S16	14	0.85	4.13	314	6.18	16	6	2	0.18	20	2	2.25	Ca-HCO_3^{-}	0.14
S17	25	1.67	2.41	358	6.80	3.42	1.53	28.54	0.05	15	17	1.25	Na-Cl	-0.43
S18	12	0.23	0.37	290	7.75	2.75	0.25	0.10	0.09	2.80	0.15	0.15	Ca-HCO_3^{-}	-1.43
S19	11	0.20	0.17	320	8.25	1.10	0.40	0.27	0.03	1.50	0.25	0.05	Ca-HCO_3^{-}	0
S20	11	0.20	0.31	318	8.01	2.50	0.50	0.11	0.07	2.50	0.45	0.08	Ca-HCO_3^{-}	-2.42

Table S1. (Continued).

Sample	As	Fe	U	Li	Cs	Rb	Sr	Ba	B	Br^-	F^-	PO_4^{3-}	NO_3^-	SiO_2	$\delta^{18}O$	δD	^{226}Ra
	μg/L									mg/L					‰		Bq/L
S1	0.44	40	0.15	ND	ND	0.47	95	47.1	17	ND	0.082	24.86	0.09	15	-8.20	-46.18	ND
S2	0.15	60	0.09	65	2.19	19	5000	2370	1070	0.80	1.66	24.86	0.04	28.03	-7.52	-48.97	0.77
S3	ND	ND	ND	1820	67.60	373	211000	54700	28100	89.54	1.67	3.32	0.29	42.80	-6.38	-56.03	59.16
S4	ND	ND	ND	346	21.10	141	37300	1400	5150	13	1.65	3.36	0.13	48	-9.47	-63.52	4.10
S5	13.4	ND	ND	309	17.50	121	28100	406	3960	13.30	1.73	7.19	0.11	54	-9.55	-66.72	1.43
S6	ND	ND	0.10	234	13.70	95.60	22300	326	3130	13.80	1.57	58.35	0.10	43	-9.22	-63.20	1.60
S7	3.91	ND	ND	1500	62.50	342	211000	39500	26900	104.87	1.36	23.11	0.54	39	-6.29	-59.20	65.08
S8	ND	ND	ND	523	24.40	133	71500	9393	8870	10	1.26	1.16	0.28	37	-8.08	-55.06	10.39
S9	1.53	50	0.24	94	3.14	17.60	1570	84	408	0.67	1.63	5.22	0.10	30	-9.07	-55.13	1.46
S10	0.07	30	ND	ND	0.08	1.71	548	37	512	ND	1.72	1.50	0.26	11	-9.89	-65.02	0.39
S11	1.03	20	1.30	ND	0.08	1.11	133	28	17	ND	0.20	9.22	0.09	10.50	-9.15	-54.81	0.45
S12	9.12	40	0.64	11	1.68	11.80	3770	38	31	0.60	2.58	3.59	3.75	24.10	-11.68	-73.56	1.56
S13	0.24	30	0.31	ND	13.70	0.13	298	38.90	11	ND	0.27	2.27	0.10	11.30	-10.50	-67.75	0.30
S14	0.31	40	0.40	ND	62.50	342	229	15.60	10	ND	0.24	8.04	0.05	6.40	-11.20	-69.86	ND
S15	164	90	0.06	1490	166	364	5000	51.70	5000	1.02	0.83	6.62	0.28	148.50	-10.91	-67.07	0.70
S16	476	44	0.74	ND	23.20	85	3730	37.60	1790	ND	0.37	1.92	0.20	99.50	-10.86	-67.35	ND
S17	3.91	70	0.90	1070	53.50	145	3660	27.10	3590	0.90	0.04	0.75	0.13	180.80	-10.37	-64.55	ND
S18	1.08	40	0.94	ND	0.02	1.82	154	55	12	ND	ND	5.58	0.60	6.80	-9.97	-58.03	ND
S19	0.14	30	4.02	ND	0.003	0.57	135	54.80	ND	ND	0.32	3.62	0.10	10	-9.60	-58.36	ND
S20	0.93	36	0.94	ND	ND	1.02	196	46.40	30	ND	0.18	3.99	0.09	7	-10.28	-60.12	0.32

Table S2. Calculated saturation index values of minerals in springs of the study area.

	Station	Aragonite	Calcite	Dolomite	Magnesite	Barite	Alstonite	Witherite	Celestite	Strontianite	Halite	Gypsum	Anhydrite	Quartz	Chalcedony	Amorph
		$CaCO_3$	$CaCO_3$	$CaMg(CO_3)_2$	$MgCO_3$	$BaSO_4$	$BaCa(CO_3)$	$BaCO_3$	$SrSO_4$	$SrCO_3$	NaCl	$CaSO_4 \cdot 2H_2O$	$CaSO_4$	SiO_2	SiO_2	SiO_2
Na-Cl water type	S2	-0.13	0.15	0.49	-0.40	-0.45	-	-	-3.10	-	-4.26	-3.37	-3.73	0.34	-0.09	-0.99
	S3	0.99	1.28	1.95	-0.09	1.11	-	-	-1.16	-	-2.90	-1.56	-1.86	0.54	0.12	-0.77
	S4	0.66	1	1.65	-0.28	0.40	-	-	-0.8	-	-2.92	-1.19	-1.27	0.27	-0.10	-0.92
	S5	0.46	0.78	1.26	-0.40	-0.08	-	-	-0.97		-2.81	-1.26	-1.43	0.43	0.04	-0.80
	S6	0.36	0.68	1.21	-0.35	-0.38	-	-	-1.28	-	-3.17	-1.42	-1.59	0.32	-0.06	-0.90
	S7	0.14	0.42	0.51	-0.65	0.96	-	-	-1.28	-	-1.38	-1.80	-2.09	0.65	0.21	-0.68
	S8	0.70	1	1.13	-0.68	0.06	-	-	-1.85	-	-2.43	-2.19	-2.43	0.39	-0.02	-0.89
	S9	0.44	0.72	1.38	-0.10	-0.31	-1.49	1.63	-2.93	0.42	-4.78	-1.63	-1.97	0.33	-0.09	-0.98
	S12	-2.19	-1.90	-3.09	-1.95	0.13	-	-	-0.88	-	-5.91	-1.84	-2.17	0.61	0.01	-0.70
	S15	0.20	0.48	0.43	-0.81	-0.01	-	-	-1.01	-	-5.06	-0.95	-1.28	1.03	0.60	-0.28
	S17	-0.18	0.10	-0.09	-0.95	-0.85	-	-	-0.67	-	-5.04	-2.10	-2.43	1.11	0.69	-0.20
$Ca\text{-}HCO_3$ water type	S1	-0.30	-0.18	0.06	-1.46	-1.03	-2.47	1.41	-5.05	-0.93	-9.22	-3.16	-3.46	0.34	0.06	-1.04
	S10	2.40	2.54	5.44	1.20	-1.15	1.77	2.96	-4.28	1.78	-6.09	-2.52	-2.82	0.14	-0.14	-1.24
	S11	0.26	0.41	1.44	-0.66	-1.47	-1.62	1.68	-5.11	-0.29	-8.17	-3.29	-3.58	0.18	-0.10	-1.20
	S13	0.30	0.44	1.45	-0.70	-1.29	-1.41	1.84	-4.76	0.06	-8.84	-3.23	-3.54	0.25	-0.03	-1.14
	S14	0.63	0.77	2.46	0.01	-1.56	-1.03	1.92	-4.55	0.59	-9.74	-3.28	-3.55	-0.10	-0.38	-1.45
	S16	-0.12	0.02	0.75	-0.97	-0.06	-2.95	0.74	-2.39	0.08	-6.79	-1.32	-1.61	1.15	0.87	-0.22
	S18	0.09	0.24	0.55	-1.38	-0.64	-1.63	1.84	-4.5	-0.35	-9.52	-2.79	-3.08	-0.01	-0.30	-1.39
	S19	-0.08	0.07	0.80	-0.98	-0.99	-3.07	1.07	-3.84	0.35	-9.06	-3.58	-3.90	0.21	-0.07	-1.19
	S20	0.20	0.35	1.10	-0.97	-0.92	-1.33	2.01	-4.84	-0.21	-8.83	-3.10	-3.43	0.08	-0.20	-1.32

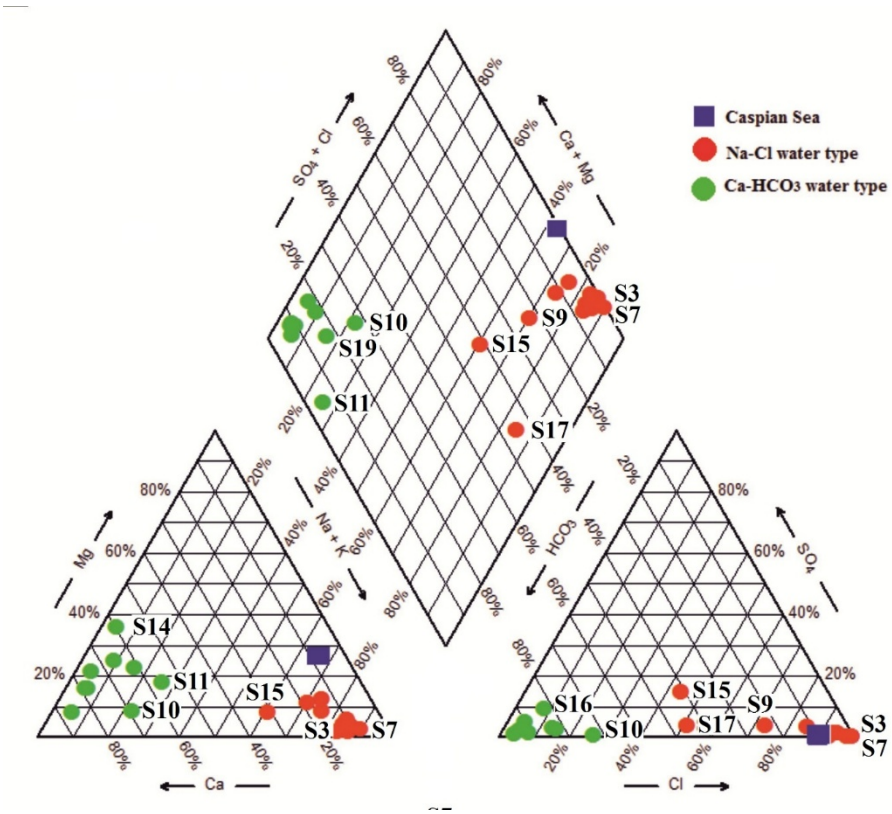

Fig. S1. Piper diagram showing the hydrochemical classification of springs water (red and green circles represent Na-Cl thermal and Ca-HCO_3 non-thermal springs, respectively, and blue square represents Caspian Sea water composition along the Southern coast (Tuzhilkin *et al.* 2005).

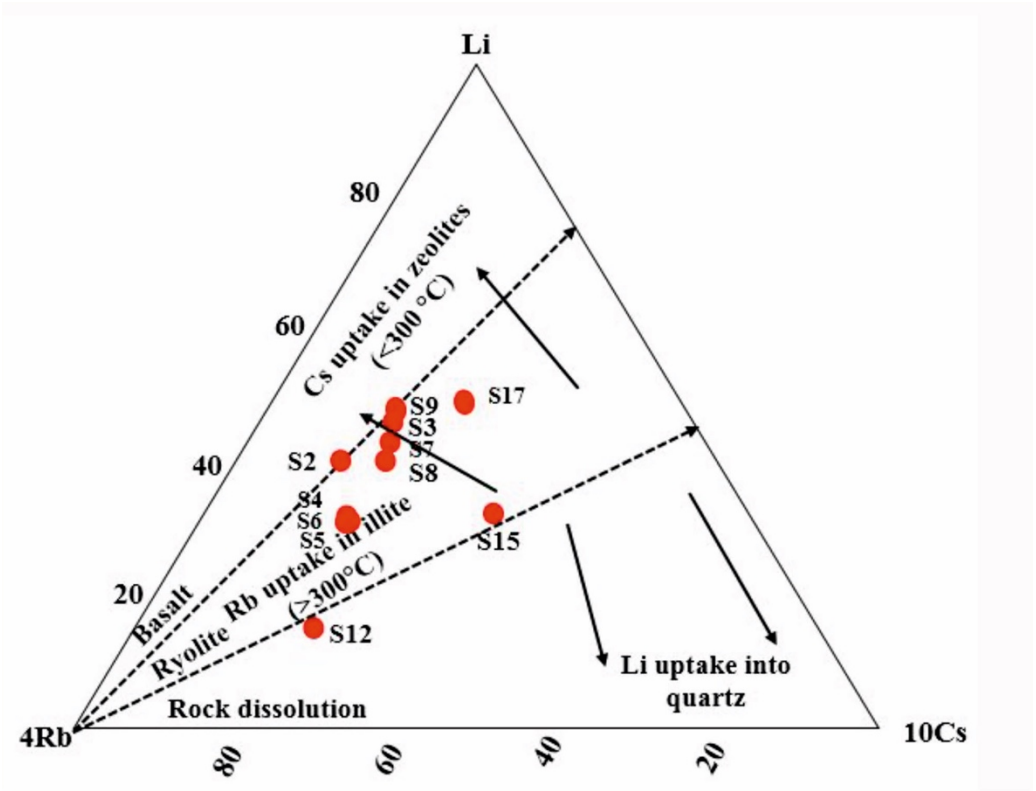

Fig. S2. Relative concentrations of Li, Rb, and Cs in thermal springs water (Giggenbach 1991).